ijndes
Published by Global Research Publications, New Delhi, India

NON-LINEAR EFFECTS OF SUSPENSION ON HUNTING AND CRITICAL VELOCITY OF RAILWAY WHEELSET

Mahmoud Shariati*, A.K.Mohammadi & N.Ale Ali
Mechanical Department, Shahrood University of Technology, Shahrood, Iran

Received: 11th January 2016, Accepted: 12th March 2016

Abstract: *In this paper the effects of non-linearity of suspension on dynamic behavior of a railway wheelset has been studied. This wheelset has four degrees of freedom with two constraints. Therefore, the degrees of freedom has reduced to two. The Vermeulen-Johnson theory has been used to calculate contact forces between wheel and rail. In this study, the creep coefficients have considered constant. Any linearization has not been used for obtaining motion equations. Lateral suspension for these wheelset is dry friction which has been modeled by using Kolesch theory. The Runge-kutta method has been used for solving these equations and results have been presented to obtain limit cycles due to hunting behavior of wheelset.*

Keywords: *Railway Wheelset, Limit Cycle, Hunting, Critical Velocity*

1. INTRODUCTION

The meaning of stability can be explained easily with this wheelset motion. Stability means that for a slight lateral displacement or yaw angle the wheelset moves back into its central position with a damped oscillatory parasitic motion. The wheelset motion is considered to be unstable if for some small irregularities an excited vibration takes place, so that the maximum amplitudes increase and the parasitic motion is finally only restricted by flange contact. As the geometrical and physical relations of contact mechanics are extremely nonlinear, attempts were made to integrate these nonlinearities at least approximately into the stability analysis. The term of "critical speed" that has used in this paper, refers to the minimum speed of the vehicle for a given set of system parameters and suspension characteristics beyond which hunting appears as an undamped motion of the wheelset constrained by the wheel flange and the rail. A history of vehicle stability implies a retrospective view on 150 or even 200 years [1]. The kinematic motion of a single wheelset with conical profiles has been well understood at least since Stephenson [2].

Hans True and Carsten Nordstrom Ensen investigated Cooperrider's mathematical model of a railway bogie running on a straight track due to its interesting nonlinear dynamics [3]. In

* Corresponding Author: *mshariati@shahroodut.ac.ir*

their article a detailed numerical investigation was made of the dynamics in a speed range, where many solutions existed, but only a couple of which were stable. One of them was a chaotic attractor. Mehdi Ahmadian and Shaopu Yang presented an analytical investigation of Hopf bifurcation and hunting behavior of a rail wheelset with nonlinear primary yaw dampers and wheelrail contact forces [4]. They showed that the nonlinearities in the primary suspension and flange contact contribute significantly to the hunting behavior. And they also showed that both the critical speed and the nature of bifurcation are affected by the nonlinear elements. Yabuno and Okamoto showed, by using the center manifold theory and the method of normal form, that the nonlinear characteristics of the bifurcation in a wheelset model with two degrees of freedom are governed by a single parameter, hence each nonlinear force need not be detected when examining the nonlinear characteristics [5]. Also, they proposed a method of determining the governing parameter from experimentally observed radiuses of the unstable limit cycle. Next, they experimentally investigated the variation of the parameter due to the presence of linear spring suspensions in the lateral direction and discuss the variation of the nonlinear characteristics of the hunting motion, which depends on the lateral stiffness.

In this paper, hunting problem with four degrees of freedom wheelset has been modeled. Two constrains are defined for wheelset and therefore, the degrees of freedom decreased to two. The proposed model has not been studied in dynamics of wheelset, yet. This model can be more completed by using exact definition of contact between wheel and rail. The type of suspension in this model is dry friction that has been modeled by Kolesch theory. This theory is used for modeling of suspension of some bogies such as Y25. In this research, the effect parameters in hunting and critical velocity have been studied.

2. MODELING

According to figure (1), for modeling of the wheelset, four degrees of freedom have been considered in vertical, lateral and also yaw and roll rotations. Three coordination systems, *XYZ*, *xyz* and *x'y'z'* have defined for motion of wheelset. *XYZ* is fixed and *x'y'z'* exists due to rotation of yaw around *Z* and *xyz* exists due to rotation of roll around *X*. In this condition, transformation matrix for transform the fixed coordinate on earth into the fixed coordinate on the wheelset is:

$$\begin{bmatrix} X \\ Y \\ Z \end{bmatrix} = \begin{bmatrix} \cos\psi & -\cos\varphi\sin\psi & \sin\psi\sin\varphi \\ \sin\psi & \cos\psi\cos\varphi & -\sin\varphi\cos\psi \\ 0 & \sin\varphi & \cos\varphi \end{bmatrix} \begin{bmatrix} x \\ y \\ z \end{bmatrix} \tag{1}$$

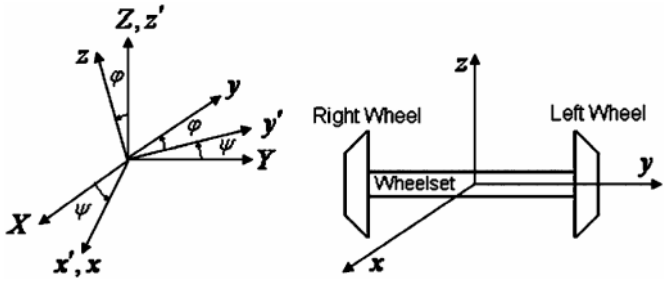

Figure 1: The Defined Coordinates for Explanation of Wheelset Movement

There are also two coordinates to define the contacts of wheelset that are shown in figure (2). The left and right contact forces are defined in left and right contact coordinate respectively. The parameters that are defined in left and right contact coordinate are determined by subscript *cl* and *cr* respectively.

It should be noticed that wheelset moves in straight line with constant velocity *V* and contact surface between wheel and rail is a point contact. Figure (2) shows details of this contact point. Wheel moves with constant velocity, so speed of rotation of its pitch rotation is constant. Thus, the angular velocity vector of wheelset can be shown as summation of three following rotational velocities.

$$\vec{\omega}_1 = \dot{\psi}\ \hat{K}\ ,\ \vec{\omega}_2 = \dot{\varphi}\ \hat{i}\ ,\ \vec{\omega}_3 = \frac{V}{r_c}\ \hat{j} \tag{2}$$

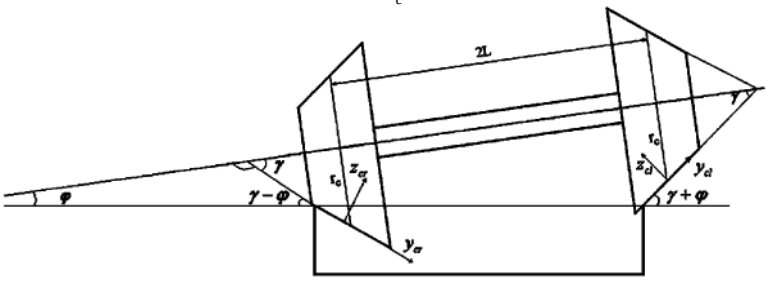

Figure 2: The Position of Wheelset on the Rail

Thus, the total angular velocity of wheelset in fixed wheelset coordinate is defined as below:

$$\vec{\omega} = \vec{\omega}_1 + \vec{\omega}_2 + \vec{\omega}_3 \ = \ \dot{\varphi}\ \hat{i}\ +\ \left(\dot{\psi}\ \sin\varphi + \frac{V}{r_c}\right)\hat{j}\ +\ \dot{\psi}\ \cos\varphi\ \hat{k} \tag{3}$$

According to figure (2), we can define two constraints for this motion that first constraint has defined according to figure (3).

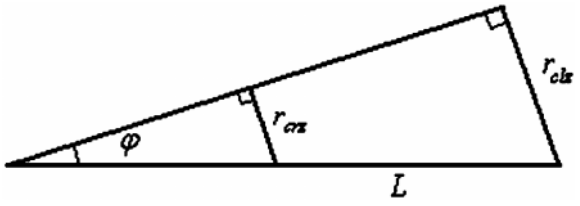

Figure 3: Roll Constrain for Wheelset's Movement

According of figure (3), we can write:

$$\sin\varphi \ = \ \frac{|r_{clz}| - |r_{crz}|}{L} \tag{4}$$

r_{clz} and r_{crz} are determined in (20) equations.

The second equation of constraint was obtained by defining five vectors. Where, vectors, $\vec{r}_1$ is distance between centre of rail and contact point, $\vec{r}_2$ is the displacement distance on the

surface of wheel as *S* due to movement of wheelset and vector $\vec{r}_3$ is distance between contact point and central of axel of wheelset. Vector $\vec{r}_G$ represents the centre of gravity of wheelset and vector $\vec{r}_4$ is defined between end of $\vec{r}_3$ and centre of gravity of wheelset. These vectors have defined in *x'y'z'* coordinate. (See figure 4)

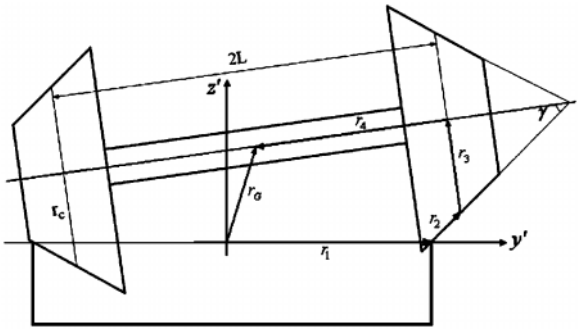

Figure 4: Relation between $\vec{r}_1$, $\vec{r}_2$, $\vec{r}_3$, $\vec{r}_4$ and $\vec{r}_G$ Vectors

$$\begin{aligned}
\vec{r}_1 &= L\,\hat{j}' \\
\vec{r}_2 &= S\left(\cos(\varphi+\gamma)\,\hat{j}' + \sin(\varphi+\gamma)\,\hat{k}'\right) \\
\vec{r}_3 &= r_c\left(-\sin\varphi\,\hat{j}' + \cos\varphi\,\hat{k}'\right) \\
\vec{r}_4 &= L\left(-\cos\varphi\,\hat{j}' - \sin\varphi\,\hat{k}'\right) \\
\vec{r}_G &= y'\hat{j}' + \left(z'+r_c\right)\hat{k}'
\end{aligned} \tag{5}$$

The relations of these vectors are shown as below:

$$\vec{r}_1 + \vec{r}_2 + \vec{r}_3 + \vec{r} = \vec{r}_G \tag{6}$$

From equation (6), the following equations are obtained:

$$\begin{aligned}
y\cos\varphi - z\sin\varphi &= L + S\cos(\varphi+\gamma) - r_c\sin\varphi - L\cos\varphi \\
y\sin\varphi + z\cos\varphi + r_c &= S\sin(\varphi+\gamma) + r_c\cos\varphi - L\sin\varphi
\end{aligned} \tag{7}$$

With eliminating *S* from equations(7), the final equation for second constraint is obtained as equation(8):

$$z\cos\gamma = y\sin\gamma - r_c\cos(\gamma+\varphi) + L\sin\gamma + r_c\cos\gamma - L\sin(\gamma+\varphi) \tag{8}$$

The matrices such as *T*, *T'*, *U*, *U'* and are the transformation matrices for transform the fixed wheelset coordinate to the left contact plane coordinate, the fixed wheelset coordinate to the right contact plane coordinate, the left contact plane coordinate to the fixed wheelset coordinate, and right contact plane to the fixed wheelset coordinate respectively.

For calculation of the contact forces and momentums, at first the velocity in contact point should be calculated. For example, the velocity of left side contact point, from relative velocity equation is defined as:

$$\vec{V}_{cl} = \vec{V}_G + \vec{\omega}\times\vec{r}_{cl} \tag{9}$$

Where

$$\vec{V}_G = V\,\hat{I} + \dot{y}\,\hat{j} + \dot{z}\,\hat{k} \tag{10}$$

Therefore, the velocity of left side contact point is calculated as below:

$$\begin{aligned}\vec{V}_{cl} = &\left(V + \left(\left(\dot{\psi}\,\sin\varphi + \frac{V}{r_c}\right)r_{clz} - \dot{\psi}\cos\varphi r_{cly}\right)U_{11} + \left(\dot{y} - \dot{\varphi}r_{clz}\right)U_{21} + \left(\dot{z} + \dot{\varphi}r_{cly}\right)U_{31}\right)\hat{i}_{cl} \\ &+ \left(\left(\left(\dot{\psi}\,\sin\varphi + \frac{V}{r_c}\right)r_{clz} - \dot{\psi}\cos\varphi r_{cly}\right)U_{12} + \left(\dot{y} - \dot{\varphi}r_{clz}\right)U_{22} + \left(\dot{z} + \dot{\varphi}r_{cly}\right)U_{32}\right)\hat{j}_{cl} \\ &+ \left(\left(\left(\dot{\psi}\,\sin\varphi + \frac{V}{r_c}\right)r_{clz} - \dot{\psi}\cos\varphi r_{cly}\right)U_{13} + \left(\dot{y} - \dot{\varphi}r_{clz}\right)U_{23} + \left(\dot{z} + \dot{\varphi}r_{cly}\right)U_{33}\right)\hat{k}_{cl}\end{aligned} \tag{11}$$

The obtaining of velocity of right side contact is similar to left one.

Also, the rotational velocity in the left contact point coordinate is defined as following equation:

$$\begin{aligned}\vec{\omega}_{cl} = &\left(\dot{\varphi}\,U_{11} + \left(\dot{\psi}\,\sin\varphi + \frac{V}{r_c}\right)U_{21} + \dot{\psi}\,\cos\varphi U_{31}\right)\hat{i}_{cl} + \left(\dot{\varphi}U_{12} + \left(\dot{\psi}\,\sin\varphi + \frac{V}{r_c}\right)U_{22} + \dot{\psi}\,\cos\varphi U_{32}\right)\hat{j}_{cl} \\ &+ \left(\dot{\varphi}U_{13} + \left(\dot{\psi}\,\sin\varphi + \frac{V}{r_c}\right)U_{23} + \dot{\psi}\,\cos\varphi U_{33}\right)\hat{k}_{cl}\end{aligned} \tag{12}$$

According to above equations, dynamics creep of wheelset is defined as below:

$$\begin{aligned}\xi_x &= \frac{V_{cx}}{V} \\ \xi_y &= \frac{V_{cy}}{V} \\ \xi_s &= \frac{\omega_{cz}}{V}\end{aligned} \tag{13}$$

In these equations, creep coefficients are assumed constant (f_{11}, f_{22}, f_{12}, f_{33}) and creep forces are obtained as below relations:

$$\begin{aligned}F'_{cx} &= -f_{33}\xi_x \\ F'_{cy} &= -f_{11}\xi_y - f_{12}\xi_{sp} \\ M'_{cz} &= f_{12}\xi_y - f_{22}\xi_{sp}\end{aligned} \tag{14}$$

These forces are assumed as limit factors and the limitation condition is defined according as:

$$\beta = \frac{1}{\mu N}\sqrt{F'^2_{cx} + F'^2_{cy}}$$

$$\varepsilon = \begin{cases} \frac{1}{\beta}\left(\beta - \frac{\beta^2}{3} + \frac{\beta^3}{27}\right) \text{For} \beta < 3 \\ \frac{1}{\beta} \text{For} \beta \geq 3 \end{cases} \quad (15)$$

Therefore, the contact forces and momentums are defined as[6]:

$$\begin{aligned} F_{cx} &= \varepsilon F'_{cx} \\ F_{cy} &= \varepsilon F'_{cy} \\ M_{cz} &= \varepsilon M'_{cz} \end{aligned} \quad (16)$$

In this article, the contact force due to nonlinear spring which has dead band was simulated. This modeling is expressed as following mathematical relation:

$$F_T = \begin{cases} -K_T\left(y - \delta\right) & y > \delta \\ 0 & -\delta < y < \delta \\ K_T\left(y + \delta\right) & y < -\delta \end{cases} \quad (17)$$

In this equation, K_T and δ are stiffness of rail and clearance of wheel flange factors respectively. Figure (5) shows the clearance of flange that is the dead band between wheel and rail [4].

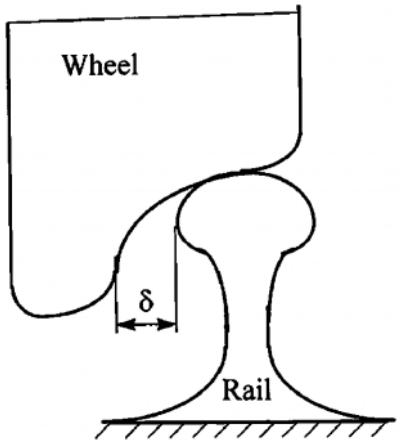

Figure 5: The Clearance and the Lateral Distance between Wheel and Rail [4]

Also, for suspending in lateral direction, nonlinear suspension has been used that utilizes in freight bogies Y25. In this condition, Kolesch's method[7] has been used for modeling as following(see section 3) :

$$\begin{aligned} C_0 &= C_h - C_g \\ \dot{K} &= C_0 \dot{y}\left(1 - 0.5\left(sign\left(\dot{y}K\right) + 1\right)\left|\frac{2K}{H}\right|^n\right) \\ F_{sus} &= C_g y + K \end{aligned} \quad (18)$$

According to modified Euler equations, equations of motion can be written as below [8]:

$$\begin{aligned} m\ddot{y} &= F_{clx}T_{12} + F_{cly}T_{22} + F_{crx}T'_{12} + F_{cry}T'_{22} + N_{cl}T_{32} + N_{cr}T'_{32} + mg\sin\varphi - F_{sus} + F_T \\ m\ddot{z} &= F_{clx}T_{13} + F_{cly}T_{23} + F_{crx}T'_{13} + F_{cry}T'_{23} + N_{cl}T_{33} + N_{cr}T'_{33} + mg\cos\varphi \end{aligned} \quad (19)$$

$$I_{xx}\ddot{\varphi} + \dot{\psi}^2\sin\varphi\cos\varphi\left(I_{zz} - I_{yy}\right) - I_{yy}\dot{\psi}\cos\varphi\frac{V}{r_c} = r_{cly}\left(F_{clx}T_{13} + F_{cly}T_{23}\right) - r_{clz}\left(F_{clx}T_{12} + F_{cly}T_{22}\right)$$

$$+r_{cry}\left(F_{crx}T'_{13} + F_{cry}T'_{23}\right) - r_{crz}\left(F_{crx}T'_{12} + F_{cry}T'_{22}\right) + N_{cl}\left(r_{cly}T_{33} - r_{clz}T_{32}\right)$$

$$+ N_{cr}\left(r_{cry}T'_{33} - r_{crz}T'_{32}\right) + M_{cl}T_{31} + M_{cr}T'_{31}$$

$$I_{zz}\left(\ddot{} \cos\varphi - \dot{} \dot{\varphi}\sin\varphi\right) - _{xx}\dot{\psi}\dot{\varphi}\sin\varphi = -_{cly}\left(_{clx\ 11} + _{cly\ 21}\right) - _{cry}\left(_{crx\ 11}' + _{cry\ 21}'\right)$$

$$-r_{cly}T_{31}N_{cl} - r_{cry}T'_{31}N_{cr} + M_{cl}T_{33} + M_{cr}T'_{33}$$

Where:

$$\begin{aligned} r_{clz} &= -(r_c + S\sin\gamma) \\ r_{cly} &= L - S\cos\gamma \\ r_{crz} &= -r_c + S\sin\gamma \\ r_{cry} &= -(L + S\cos\gamma) \end{aligned} \quad (20)$$

3. LATERAL SUSPENSION

For suspension modeling of some freight bogies (Y25), a special kind of friction damper has been used. Figure (6) shows the mechanical model of this force element [9].

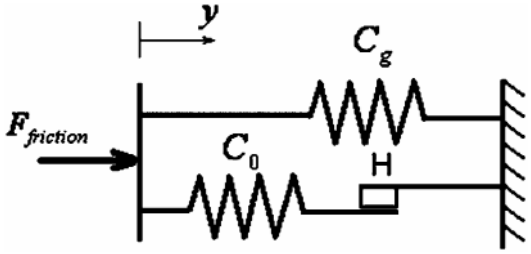

Figure 6: Mechanical Model of Kolesch's Friction Damper Elements

This model contains a series spring connection with stiffness C_0 and a frictional damper with damping force H. This spring and frictional damper have been jointed with another spring with stiffness C_g as parallel. When there is a displacement in y direction(extension or compression), the spring C_0 will deform until the damper force H is fully created. So the system is actions similar to a single spring which total stiffness C_h:

$$C_h = C_0 + C_g \quad (21)$$

If the generated force by spring (C_0) is more than the maximum damper force, the frictional part of system starts to slide and friction force is generated opposite to direction of motion. The total amount of friction force is defined as below:

$$F_{\text{friction}} = C_g y + K \quad (22)$$

In this relation, K is the existed force in frictional part that is defined as:

$$\dot{K} = C_0 \dot{y} \left\{ 1 - 0.5\left(1 + sign\left(\dot{y}K\right)\right) \left| \frac{K}{H} \right|^n \right\} \tag{23}$$

In this stage two different conditions are modeled:

a. The damper force is constant and the maximum amount of H is defined as:

$$H = \mu_s \cdot F_{Normal} \tag{24}$$

b. The damper force is not constant and it is variable as following equation that names as force dependent.

$$H = \mu_s \left(F_{Preload} + C_g y + K \right) \tag{25}$$

$F_{Preload}$ is the force that is considered as preload frictional force. In this article, the first condition of Kolesch's theory is considered.

If we apply the sinusoidal displacement on this force element, we obtain hysteretic force-displacement diagram. (See figure (7)). According to figure (7), C_g is the slope of the slip motion and C_h is the slope of the stick motion in the hysteretic force-displacement diagram. n affect on the sharpness of this diagram.

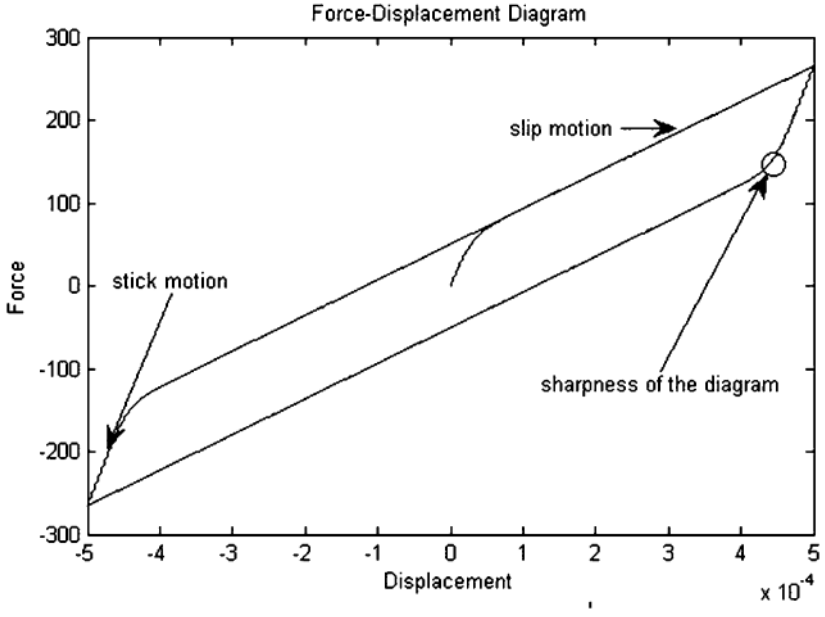

Figure 7: Hysteretic Diagram

4. SIMULATION

According to numerical values which have been shown at table (1), equations (4), (8) and (19) have been solved simultaneously by using Runge-Kutta numerical method. A bifurcation graph for this dynamical system has drawn in figure (8). Critical velocity of wheelset is considered 33 m/s in these conditions. Also behavior of wheelset compare to lateral displacement has been

shown in figure (9). Figure (10) shows the limit cycle behavior. This behavior is defined as hunting phenomena. With increasing the velocity, then limit cycle will appear. While velocity is smaller than critical velocity, then there is no limit cycle and wheelset will return to equilibrium or central position. Figure (11) and (12) show these behaviors. It should be mentioned that initial displacement was 8 millimeters.

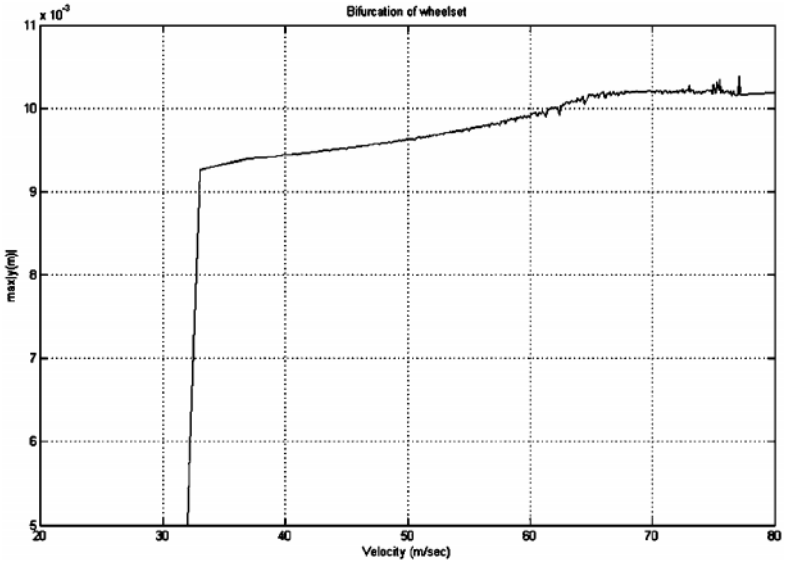

Figure 8: Bifurcation of Wheel vs. the Velocity Curve

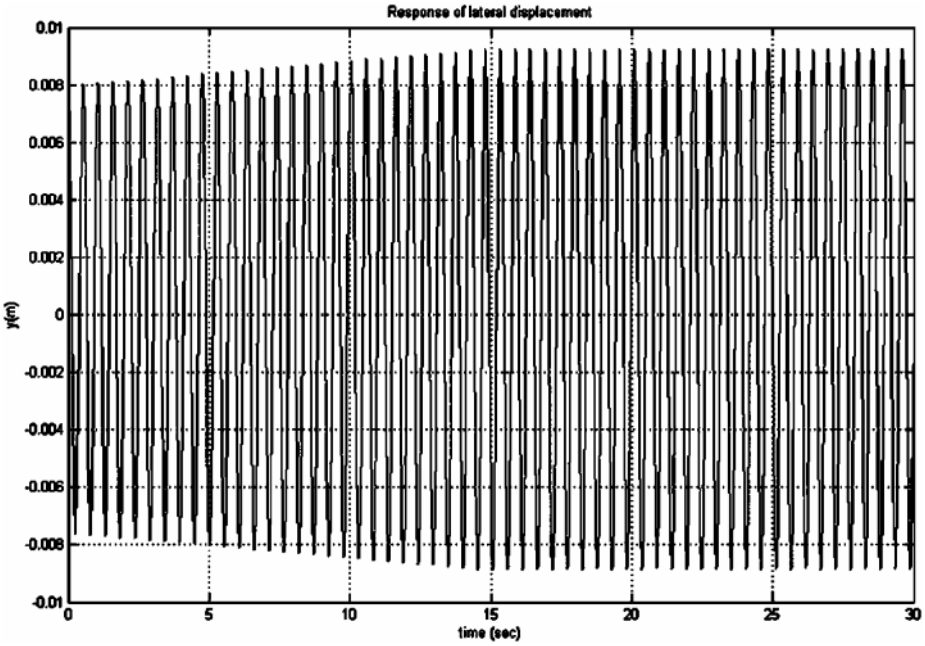

Figure 9: Lateral Displacement Graph of Wheelset at Critical Velocity (Hunting)

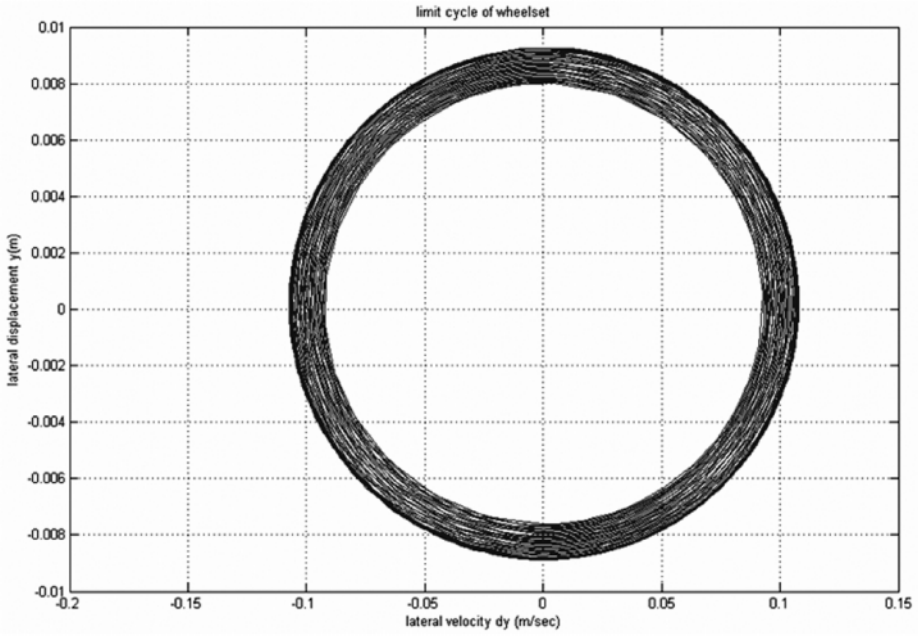

Figure 10: Limit Cycle Graph of Wheelset at Critical Velocity (Hunting)

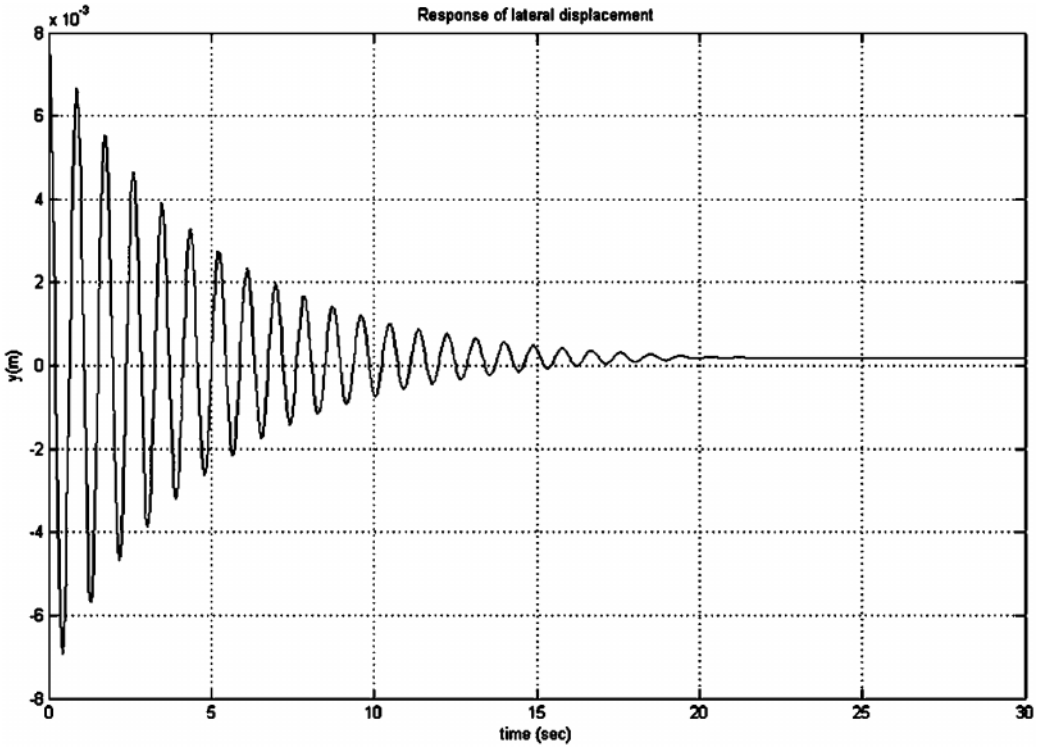

Figure 11: Lateral displacement graph of wheelset at v = 20 m/s

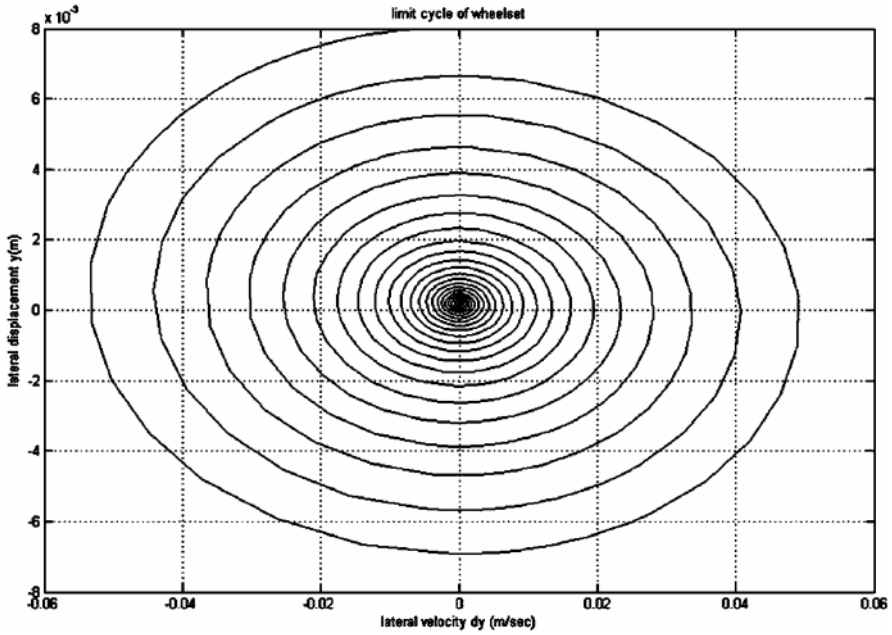

Figure 12: Limit Cycle Graph of Wheelset at v = 20 m/s

5. RESULTS AND DISCUSSION

In this section, nonlinear characteristics of suspension are investigated. While the stiffness of spring C_g =107500 N/m, then critical velocity is equal to 15.7 m/s and limit cycle in terms of velocity has been shown in figure (13).

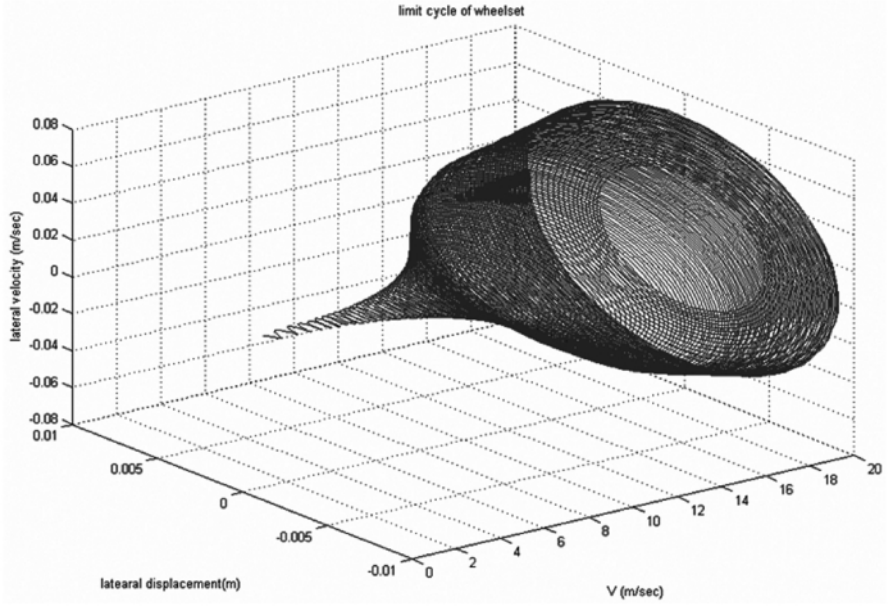

Figure 13: Limit Cycle for C_g =107500 N/m

Figure (14) shows critical velocity when C_g = 215000 N/m, also figure (15) shows limit cycle in terms of velocity when C_g = 537500 N/m and critical velocity is equal to 36.5 m/s.

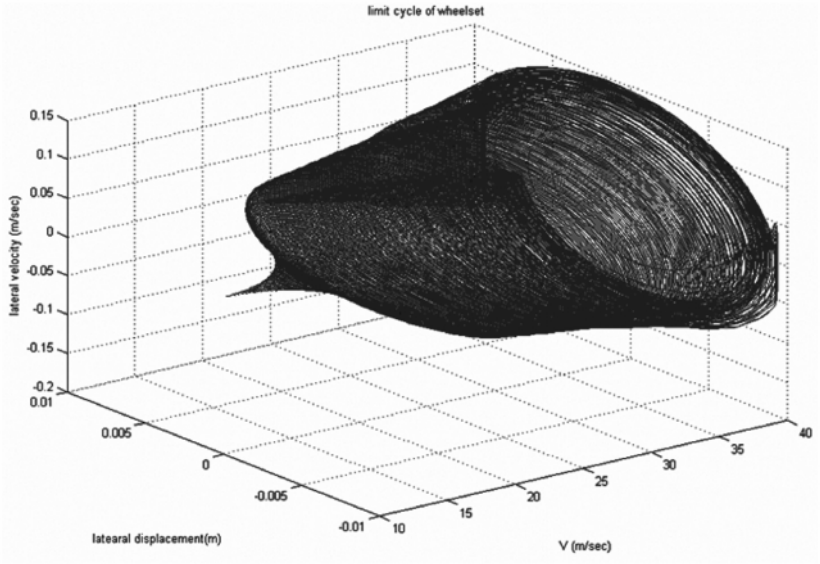

Figure 14: Limit Cycle when C_g = 215000 N/m

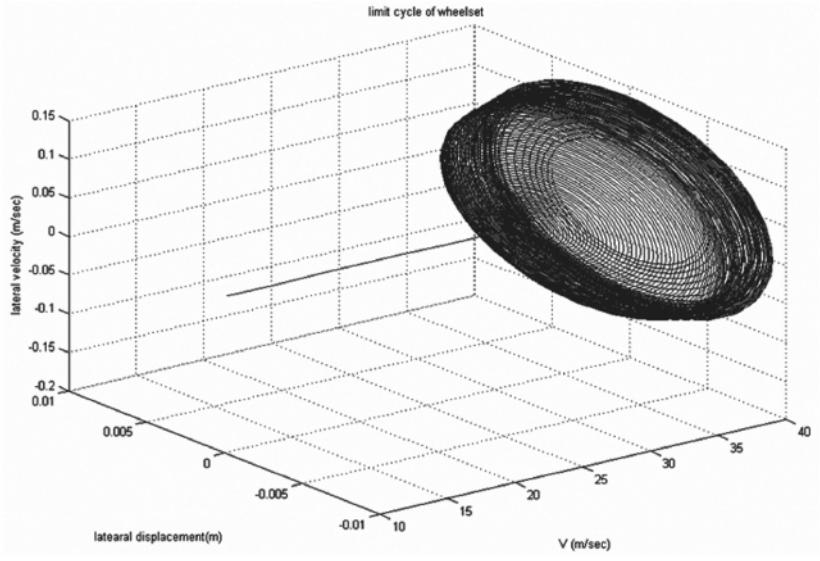

Figure 15: Limit cycle when C_g = 537500 N/m

Figure (16) shows limit cycle in terms of velocity when C_g = 645000 N/m and critical velocity is equal to 40.1 m/s.

As results show, with increasing the C_g, critical velocity is increased. But there are limitation in increasing the value of C_g. The limitation of increasing of C_g is the increasing of frequency of oscillation of wheelset.

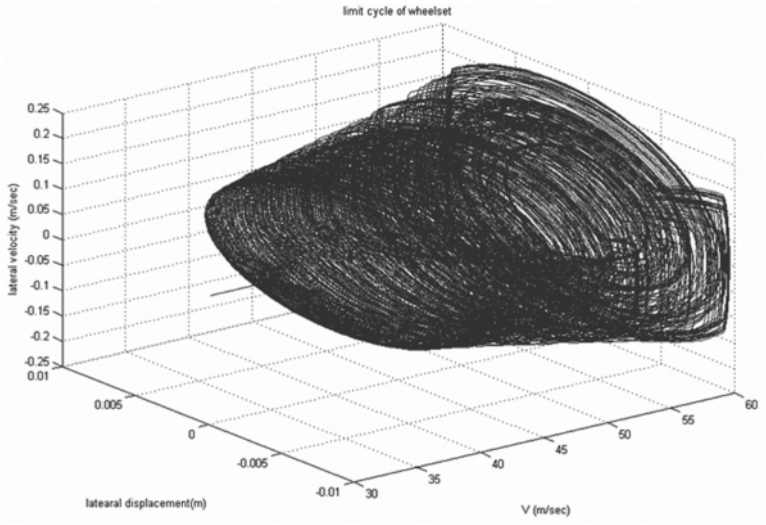

Figure 16: Limit Cycle when C_g = 645000 N/m

For analyzing the variations of damper forces (H), three different cases are considered that critical velocity has been investigated according to figure (17). H depends on kinetic friction coefficient of sliding surfaces of suspension system and weight of wheelset and the load that is applied to axle of wheelset. Variation of the kinetic friction coefficient is small. The variation of axle load of wheelset is more affected on value of H. Therefore the empty wagon is more critical than the full wagon in view of velocity.

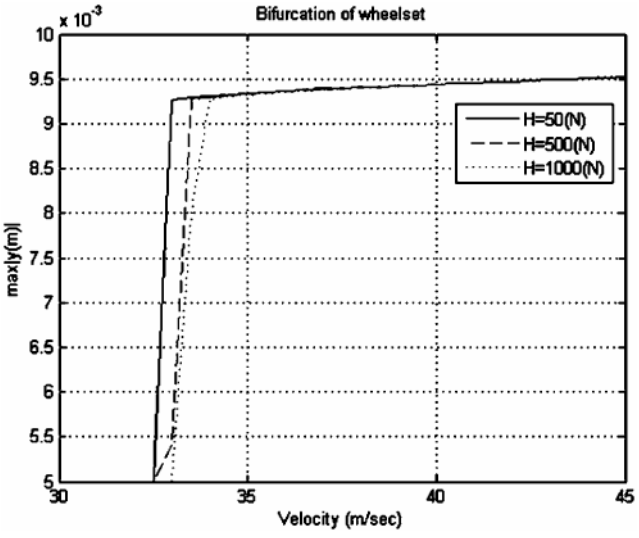

Figure 17: Bifurcation Graph for Three different Values of Dry Friction Damper Force

5. CONCLUSION

With increasing the values of H and C_g, the critical velocity of wheelset will rise, but the effect of C_g on increasing of critical velocity is more than H. Therefore, the increase of slipping dry

friction coefficient or axial load of wheelset will not change the critical velocity as an important dynamical parameter of wheelset. Also when velocity is more than critical velocity, the limit cycle will appear and in this condition, there is an attractor in system.

Table 1
The Values of Wheel Set's Constants [4, 6, 7]

m	Mass of wheelset	1800 kg
I_{xx}	roll moment of inertia of the wheelset	625.7 kg.m^2
I_{yy}	pitch moment of inertia of the wheelset	133.92 kg.m^2
r_c	Nominal weelset rolling radius	0.533 m
γ	Wheel conicity	0.05
L	Half of track gauge	0.7176 m
f_{11}	Lateral creep force coefficient	6.728×10^6
f_{12}	Lateral/spin creep force coefficient	1200
f_{22}	Spin creep force coefficient	1000
f_{33}	Longitudinal creep force coefficient	6.728×10^6
μ	Friction coefficient	0.3
g	Acceleration of gravity	9.81 m/s^2
K_T	Lateral rail stiffness	1.617×10^8 N/m
δ	flange clearance between the wheel andthe rail	0.00923 m
C_h	Stiffness of the suspension in slide motion	2.2×10^6 N/m
C_g	Stiffness of the suspension in stick motion	4.3×10^5 N/m
H	Damping dry friction force	50 N
n	The parameter denoting the sharpness of the hysteretic force-displacement diagram of the force element of the suspension	2
V	Forward velocity of wheelset	
S	displacement distance on the surface of wheel due to movement of wheelset	
r_{clz}	z component of vector that is defined from center of gravity of wheelset to left contact point	
r_{cly}	y component of vector that is defined from center of gravity of wheelset to left contact point	
r_{crz}	z component of vector that is defined from center of gravity of wheelset to right contact point	
r_{cry}	y component of vector that is defined from center of gravity of wheelset to right contact point	
F_T	flange force	
N	normal force of wheelset	
F_{cl}	Left contact force	
F_{cr}	Right contact force	
M_{cl}	Left contact moment	
M_{cr}	Right contact moment	

REFERENCES

[1] K. Knothe and F. Böhm, "History of Stability of Railway and Road Vehicles", *Vehicle System Dynamics, 31-1999., pp. 283–323.*

[2] Wickens, "The Dynamics of Railway Vehicles - from Stephenson to Carter", In *Proceedings of the Conference "From Rocket to Eurostar and Beyond", Held at the National Railway Museum London on 5 November 1997*.

[3] C. N. Jensen and H. True, *"On a New Route to Chaos in Railway Dynamics", Nonlinear Dynamics,* **13**: 117-129, 1997.

[4] M. Ahmadian and S. Yang, "Hopf Bifurcation and Hunting Behavior in a Rail Wheelset with Flange Contact*", Nonlinear Dynamics,* **15**: 15-30, 1998.

[5] H. Yabuno, T. Okamoto and N. Aoshima, "*Effect of Lateral Linear Stiffness on Nonlinear Characteristics of Hunting Motion of a Railway Wheelset",* Meccanica, **37**: 555-568, 2002.

[6] A. Mohan and M. Ahmadian, *"Nonlinear Investigation of the Effect of Primary Suspension on the Hunting Stability of a Rail Wheelset", Proceeding of the 2004 ASME/IEEE Joint Rail Conference*.

[7] H. Molatefi, M. Hecht and M. H. Kadivar, "Critical Speed and Limit Cycles in the Y-25 Freight Wagon"*, Proc. IMechE,* **220**, Part F: J. Rail and Rapid Transit. 2006.

[8] H. Baruh, 1999, "Analytical Dynamics", *WBC/McGraw-Hill.*

[9] S. Y. Lee and Y. C. Cheng, "Hunting Stability Analysis of High-speed Railway Vehicles Trucks on Tangent Tracks", *Journal of Sound and Vibration,* **282** (2005) 881–898.